



Threshold voltage decrease in a thermotropic nematic liquid crystal doped with graphene oxide flakes

Mateusz Mrukiewicz^{*1}, Krystian Kowiorski², Paweł Perkowski¹, Rafał Mazur¹ and Małgorzata Djas²

Full Research Paper

Open Access

Address:

¹Institute of Applied Physics, Military University of Technology, 00-908 Warsaw, Poland and ²Department of Chemical Synthesis and Flake Graphene, Institute of Electronic Materials Technology, 01-919 Warsaw, Poland

Email:

Mateusz Mrukiewicz* - mateusz.mrukiewicz@wat.edu.pl

* Corresponding author

Keywords:

graphene oxide; liquid crystal; nematic phase; switching; threshold voltage

Beilstein J. Nanotechnol. **2019**, *10*, 71–78.

doi:10.3762/bjnano.10.7

Received: 23 July 2018

Accepted: 30 November 2018

Published: 07 January 2019

Associate Editor: S. A. Claridge

© 2019 Mrukiewicz et al.; licensee Beilstein-Institut.

License and terms: see end of document.

Abstract

We report a threshold voltage decrease in a nematic liquid crystal compound, 4-cyano-4'-pentylbiphenyl (5CB), doped with graphene oxide (GO) flakes at a concentration of 0.05–0.3 wt %. The threshold voltage decrease was observed at the same concentration in electro-optic and dielectric spectroscopy measurements. The effect is related to the disrupted planar alignment due to the strong π - π stacking between the 5CB's benzene rings and the graphene oxide's structure. Additionally, we present the GO concentration dependence on the isotropic–nematic phase transition temperature, electric anisotropy, splay elastic constant, switch-on time, and switch-off time. The shape and dimensions of the GO flakes were studied using atomic force microscopy (AFM) and scanning electron microscopy (SEM). The influence of the GO concentration on the physical properties and switching process in the presence of the electric field was discussed.

Introduction

Liquid crystals (LCs) are classified as a type of soft matter which are characterized by anisotropic molecules and a liquid-like fluidity behavior. Of all LC phases, special attention is paid to the nematic liquid crystal (NLC) phase because it is widely used in many electro-optical applications [1,2]. In the uniaxial nematic phase, the direction of the optical axis is described by the director \mathbf{n} , which is the unit vector along the molecular axis. An applied electric field can change the director orientation

thereby causing a change in the optical properties. In the absence of an electric field, the orientation of \mathbf{n} is determined by anchoring conditions. The field-induced reorientation of the LC director is known as the Fréedericksz effect [3]. In the Fréedericksz effect, the deformation of a homogeneous layer of a NLC is caused by the electric field \mathbf{E} , which is initially perpendicular to the director. Such structural transition appears at a certain magnitude called the threshold voltage, U_{th} . When the

applied voltage, U , is lower than the threshold $U < U_{\text{th}}$ the tilt angle θ is small. When the voltage is above U_{th} , we start to observe the increase of θ [4]. The complete reorientation of the director \mathbf{n} , $\theta = 90^\circ$, occurs at higher voltages $U > U_{\text{th}}$. The reorientation is caused by the anisotropy of the electric permittivity $\Delta\varepsilon = \varepsilon_{\parallel} - \varepsilon_{\perp}$, where ε_{\parallel} and ε_{\perp} is the electric permittivity measured along the directions parallel and perpendicular to \mathbf{n} , respectively. In the case of positive electric anisotropy ($\Delta\varepsilon > 0$), the director is forced to align along the electric field.

One of the most efficient methods to reduce the threshold voltage in nematic liquid crystals for high electro-optical performance is doping them with nanoparticles. Hsu et al. showed that the small addition of gold nanoparticles decreases U_{th} due to the increased electric anisotropy and decreased elastic constant [5]. Haraguchi and collaborators doped the twisted nematic liquid crystal cell with inorganic nanoparticles of MgO and SiO₂ [6]. Here, the effect was caused by the reduction of the order parameter S . The concentration-dependent enhancement of the electro-optic response was observed for Ti and TiO₂ nanoparticles dispersed in NLC [7,8]. The significant effect of ferroelectric Sn₂P₂S₆ on the threshold voltage was reported by Reznikov et al. [9]. Materials with a suspension of ferroelectric, submicrometer particles exhibit a lower threshold voltage and enhanced electric anisotropy compared to pure liquid crystal compounds [9,10].

Extensive research has also been performed on carbon-based material composites [11–14]. NLCs doped with graphene or carbon nanotubes show a faster response in electro-optical switching than pure liquid crystal compounds. This effect is caused by trapping of some free ion concentrations [15,16] or reduction in the rotational viscosity [17]. Furthermore, due to strong π – π electron stacking of liquid crystal molecules on graphene sheets, one obtains pseudo-nematic domains [18], which enhance the electric anisotropy in the nematic phase. Carbon nanotubes doped into the nematic liquid crystal can effectively reduce the driving voltage due to the increase of the elastic constant [19–21].

In this work, we discuss our approach in reducing the threshold voltage by using graphene oxide (GO) flakes. The extraordinary properties of GO make this material a good candidate for this purpose. GO is an oxidized form of graphene [22–24]. In GO, carbon atoms are highly decorated with various oxygen-containing groups, for instance, hydroxyl, carbonyl, carboxyl and epoxy [25]. In contrast to graphene, the oxygen groups make graphene oxide layers hydrophilic [25], negatively charged [23] and insulating. The oxidized layers are randomly distributed with non-oxidized areas. Therefore, the main advantage of GO is easy dispersibility in water and organic sol-

vents [23,25]. Graphene oxide occurs in the form of two-dimensional flakes with anisotropic properties [24]. In thermotropic nematic liquid crystals, GO flakes create dipoles due to Maxwell–Wagner polarization [26]. An applied electric field acts to induced dipole moments, which causes reorientation of the flakes [27,28]. The above-mentioned facts are very important features for mixing a nematic liquid crystal with GO flakes in order to improve its physical properties.

Here, the nematic liquid crystal compound 4-cyano-4'-pentylbiphenyl (5CB) was doped with low concentrations (0.05–0.3 wt %) of GO flakes. We found that using the GO flakes we are able to reduce the threshold voltage in the Fréedericksz effect. We report and discuss the isotropic–nematic phase transition temperature, splay elastic constant K_{11} , electric anisotropy $\Delta\varepsilon$, switch-on τ_{ON} and switch-off τ_{OFF} times and their dependence on the concentration of the GO flakes.

Materials and Methods

Graphene oxide (GO) flakes dispersed in water were obtained from natural graphite by the modified Hummers' method [29,30] in the Department of Chemical Synthesis and Flake Graphene, Institute of Electronic Materials Technology, Warsaw, Poland. Then, the GO flakes in water were transferred by solvent exchange into isopropanol (IPA) and were sonicated to achieve a stable GO-IPA suspension of a known concentration. The structure of the flakes was characterized by scanning electron microscopy (SEM, Auriga Cross Beam Workstation, Carl Zeiss). The GO flakes had an irregular two-dimensional shape (Figure 1a). Additionally, we observed that they exhibit a tendency to fold and wrinkle. In the experiment, the mean equivalent diameter of the GO flakes was 0.801 μm while the standard deviation (SD) was equal to 0.543 μm (Figure 1b). The calculations were done using ImageJ software (V. 1.52a). The thickness of the GO flake samples was measured using a MFP 3D BIO (Asylum Research/Oxford Instruments) atomic force microscope (AFM) working in semi-contact regime (Figure 2a). This technique can provide qualitative and quantitative information about tested samples [31–33]. To register topographical maps, silicon AC240 TS (Olympus) scanning probes were used in a frequency range from 0.8 to 1.0 Hz. The nominal probe spring constant was 2.7 N/m and the radius was <10 nm. The AFM examination was carried out in air, under ambient conditions. The data analysis was conducted with IgorPro (V. 6.17, professional, dedicated software provided by the microscope producer). The measured thickness was around 1–2 nm (Figure 2b), which corresponds to 2–4 single layers of graphene. After characterization by SEM and AFM, the GO-IPA suspension was added to 4-cyano-4'-pentylbiphenyl (5CB) to obtain different GO concentrations (0.05–0.3 wt %). Isopropanol was evaporated at 45 $^\circ\text{C}$ for 24 h.

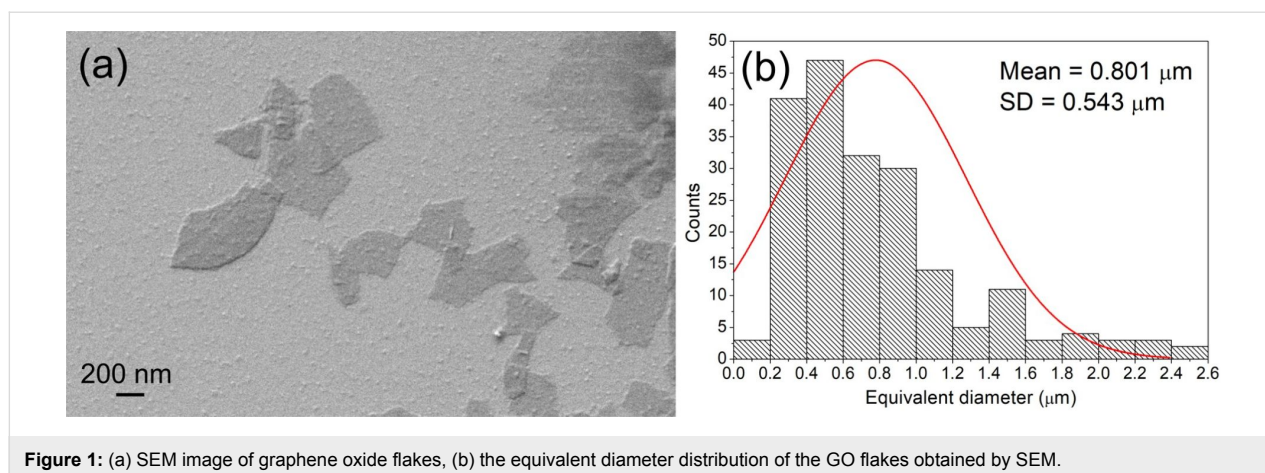


Figure 1: (a) SEM image of graphene oxide flakes, (b) the equivalent diameter distribution of the GO flakes obtained by SEM.

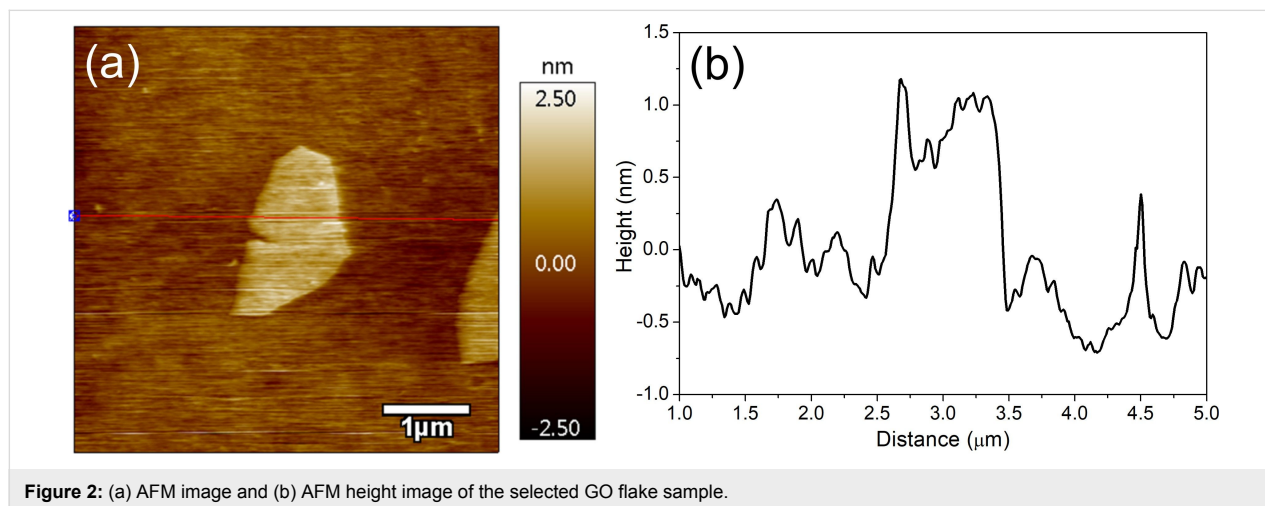


Figure 2: (a) AFM image and (b) AFM height image of the selected GO flake sample.

The rod-like 5CB compound was synthesized in the Institute of Chemistry, Military University of Technology, Warsaw, Poland. It is a room temperature nematic liquid crystal material of high chemical stability. The phase transition from the isotropic phase to the nematic phase and then to the crystalline phase is at 35 °C and 18 °C, respectively [34–36]. Pentylcyanobiphenyl (5CB) has a large longitudinal (μ_{\parallel}) electric dipole moment, which equals 6.37 D, while the transverse component (μ_{\perp}) is 0.15 D [36]. Hence, the material shows a relatively large positive electric anisotropy $\Delta\epsilon$ ($\Delta\epsilon \approx 12$ at 1 kHz and 25 °C) [34,36,37].

The nematic liquid crystal materials doped with the GO flakes were filled by capillary action into cells. The cells consisted of two pieces of parallel glass plates of thickness $d = 1.1$ mm (Precision Glas & Optik GmbH), covered by thin ($d \approx 100$ nm) ITO conducting layers, separated by 1.6 μm thick glass spacers. An active area was 25 mm². On the glass plates a polyimide SE-130 (Nissan Chemicals) of $d \approx 30$ nm was deposited and rubbed to induce planar alignment (HG, homogenous) of the

director n . The isotropic–nematic phase transition temperature was determined by means of the transmitted light intensity (TLI) technique, as a function of temperature. The temperature was controlled with a Linkam TMS 93 controller and a heating stage, THMSE 600. The intensity of light propagating through the cell under crossed polarizers, without the applied electric field, was registered with a photodetector, FLC Electronics PIN 20. The switching times were measured using the same experimental set-up. In the electro-optic (EO) experiment, the switching was driven by the ac square electric signal at a frequency of 1 kHz generated by a waveform generator, Agilent 33220A. Moreover, to determine the switching times in the electrically controlled birefringence (ECB) mode of operation, an oscilloscope (Tektronix TDS 2014) was used to register the electro-optical response. The duration of the driving pulse was 1 s. Dielectric spectroscopy (DS) studies were performed using an impedance analyzer (Agilent 4294A) and conducted over a broad frequency range from 100 Hz to 10 MHz, with the oscillation level (ac) at 0.1 V and with different (dc) bias voltages. All measurements were performed at 23 °C.

Results and Discussion

The influence of the GO flakes on the quality of alignment in the planar oriented liquid crystal cells was studied by observation of liquid crystal textures using the polarizing optical microscope (POM) technique. In the all liquid crystal composites, the GO flakes were well dispersed. The liquid crystal cells exhibited uniform color, indicating that the rod-like molecules were uniformly aligned. However, Figure 3b–e, illustrates some GO aggregation. The size and quantity of the aggregates is much more visible for the higher concentration (Figure 3e) than for the lower concentration (Figure 3b). The large aggregates disorder the long-range orientational order and disturb the liquid crystal alignment. According to the classical Michel–Levy interference color chart [38], we observe a slight decrease in birefringence of GO composites compared with the pure 5CB nematic liquid crystal (Figure 3a). For concentrations higher than 0.3 wt %, we can expect the creation of a lyotropic nematic phase in the isotropic phase of the 5CB-GO suspension, as was previously reported [39,40].

We used the TLI technique for making precise measurements of phase transition temperatures. In the case of the isotropic–nematic phase transition, in the isotropic state, the intensity of light propagating through the cell under crossed polarizers is around zero (dark state). During the cooling process, at the phase transition temperature T_{I-N} , the transmission of light starts to increase due to the nucleation of the nematic phase (bright state). In the experiment, the clearing temperature of the pure 5CB (33.0 °C) was 2 °C below that of previous reports [34,36]. The effect of the lower T_{I-N} is related to the strong boundary conditions of the thin cell. As shown in Figure 4, increasing the GO concentration up to 0.1 wt % increases the isotropic–nematic phase transition by about 0.1–0.2 °C. For concentrations higher than 0.1 wt % T_{I-N} is shifted towards lower temperatures. For example, in the 5CB-GO suspension of 0.3 wt % the phase transition temperature occurs at 32.4 °C. These results are consistent with the previous studies on the mixture of 5CB and 7CB with the addition of GO [12]. It was reported that the T_{I-N} temperature increases at lower concentrations of GO, while it decreases as the ratio is increased above

the certain value (0.75 wt %). The difference in phase transition temperatures of the 5CB-GO composites can be attributed to the different interactions between the liquid crystal molecules and the GO flakes. On the one hand, for the lower GO ratios 0.05–0.1 wt % the nematic order is enhanced by the strong π – π stacking. The π – π stacking between the 5CB molecules and the GO flakes causes the appearance of the nematic-like domains in the isotropic phase. Therefore, we observe at higher temperatures the creation of the nematic phase. On the other hand, when the concentration of GO exceeds 0.1 wt %, the GO flakes disturb the formation of the nematic phase.

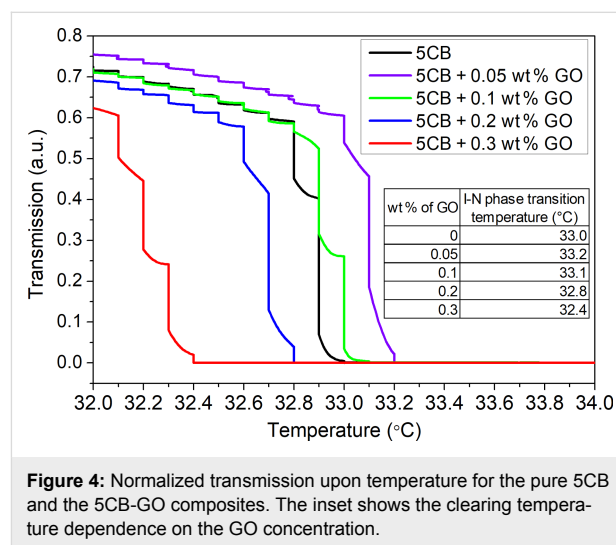


Figure 4: Normalized transmission upon temperature for the pure 5CB and the 5CB-GO composites. The inset shows the clearing temperature dependence on the GO concentration.

In this experiment, the Fréedericksz transition was induced by the electric field. The threshold voltage dependence on the GO concentration in 5CB was investigated by two methods: an electro-optic (EO) and dielectric spectroscopy (DS) experimental technique. On one hand, in EO we measure the intensity of light passing through the cell between crossed polarizers as a function of an applied voltage. On the other hand, DS is based on measurements of electric permittivity ϵ at a given frequency under different bias (dc) electric fields. These experimental techniques allowed to obtain two independent characteristics of the threshold voltage. The main difference in the above-

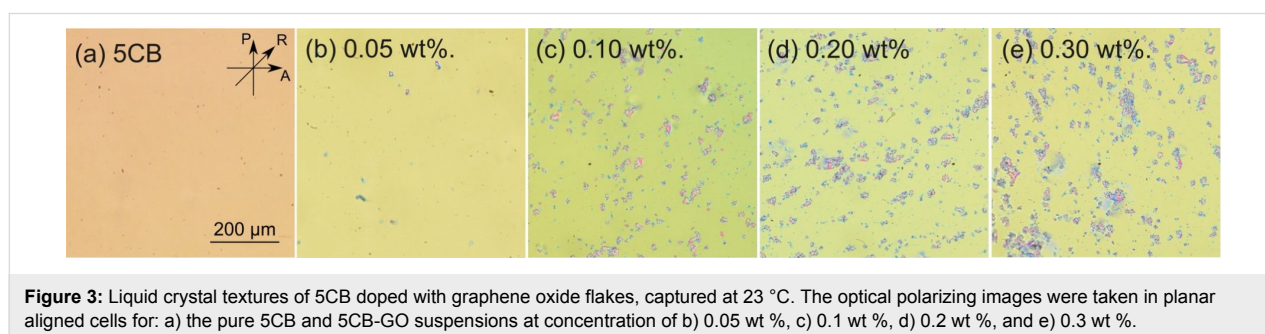


Figure 3: Liquid crystal textures of 5CB doped with graphene oxide flakes, captured at 23 °C. The optical polarizing images were taken in planar aligned cells for: a) the pure 5CB and 5CB-GO suspensions at concentration of b) 0.05 wt %, c) 0.1 wt %, d) 0.2 wt %, and e) 0.3 wt %.

mentioned methods is that in the DS measurements we are able to observe a full orientation of the director at U_{th} . In the case of the EO technique, we detect the beginning of the switching mechanism. A discrepancy is a consequence of the fact that EO measurements are carried out on a small, isolated area while in DS data are collected from a whole ITO electrode. For this reason, the values of the threshold voltage from the DS investigations (U_{th-DS}) using the bias electric field are overstated compared to the results from the EO experiment (U_{th-EO}).

Figure 5 presents the transmission of light versus the applied electric field. The U_{th-EO} in EO is defined as the voltage at which the transmission of polarized light starts decreasing. Compared to the pure 5CB, the experimental results show the increase of the threshold voltage at the concentration of 0.05 wt %. However, further increase of the GO ratio results in the opposite trend. We observe the shift of the transmission curves towards the lower voltages. The highest reduction in U_{th-EO} is observed at 0.2 wt % of GO, the threshold voltage is reduced by 10% (decrease from 0.80 V to 0.72 V).

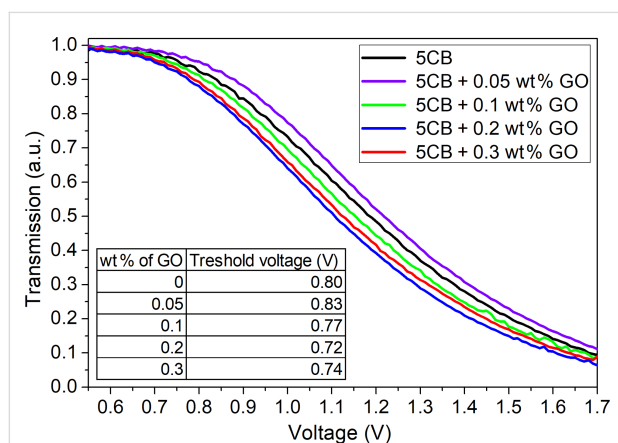


Figure 5: Normalized transmission of light as a function of applied voltage for the pure 5CB and the 5CB-GO suspensions at the different concentrations. The inset shows the threshold voltage U_{th-EO} dependence of the GO concentration.

In DS the threshold voltage U_{th-DS} is defined as the point where electric permittivity ϵ starts increasing from the initial value (perpendicular component ϵ_{\perp} of electric permittivity tensor). Thus, for the high bias voltages, we are able to determine the parallel component ϵ_{\parallel} from the plateau range of the measured electric permittivity ϵ . Figure 6 presents the electric permittivity characteristic as a function of the bias (dc) electric field. Here, we observe the decrease of U_{th-DS} at the same concentration (0.2 wt %) as in the case for the EO measurements. However, in DS, the effect of the GO flakes on the threshold voltage is much more pronounced. At a concentration of 0.2 wt %, the threshold voltage ($U_{th-DS} = 1.30$ V) is lower by almost half as

compared to the pure 5CB ($U_{th-DS} = 2.78$ V). As in the case for EO in DS we observe the increase in the threshold voltage at 0.3 wt %. The obtained values of ϵ_{\perp} and ϵ_{\parallel} in this experiment allow us to calculate the electric anisotropy $\Delta\epsilon$ of the investigated materials. The detailed results are gathered in Table 1. We found that $\Delta\epsilon$ slightly changes in the 5CB-GO composites. The highest value of $\Delta\epsilon$ is observed at 0.20 wt % ($\Delta\epsilon = 12.22$), while the lowest is at 0.05 wt % ($\Delta\epsilon = 11.77$), compared to the pure 5CB ($\Delta\epsilon = 12.04$).

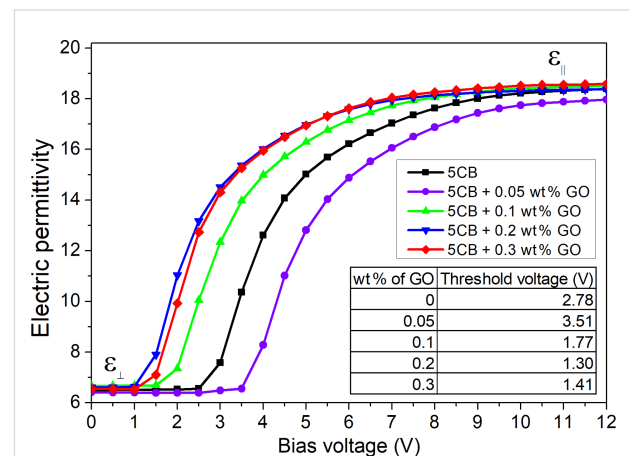


Figure 6: Electric permittivity ϵ dependence upon the bias (dc) electric field at a frequency of 1 kHz. Results obtained for the pure 5CB and the 5CB-GO suspensions at different concentrations. The inset shows the threshold voltage U_{th-DS} dependence of the GO concentration. Experimental data is presented as scattered points with the line as a guide for the eye.

Table 1: Values of the electric anisotropy $\Delta\epsilon$ in the 5CB-GO composites as a function of the GO concentration.

wt % of GO	$\Delta\epsilon$ (1 kHz, 25 °C)
0	12.04
0.05	11.77
0.1	11.96
0.2	12.22
0.3	12.05

Knowing the threshold voltage U_{th-EO} from the EO measurements and the electric anisotropy $\Delta\epsilon$ of the GO composites one can calculate the elastic constants, K_{11} values, from the formula: $U_{th} = \pi\sqrt{K_{11}/(\epsilon_0\Delta\epsilon)}$. The elastic constant is a parameter characterizing the elastic interaction between the nematic molecules. However, when GO flakes are inserted in the cell, the value of K_{11} of the 5CB-GO composites also reflects the interaction between the molecules and the inserted GO flakes [41,42]. In Table 2 we see that the threshold voltage behavior of the 5CB-GO suspensions is reflected in the concentration dependence of K_{11} . The small amount (0.05 wt %) of the carbon

dopant leads to deterioration of properties relevant for liquid crystal applications. This is due to the increase of U_{th} and K_{11} and the decrease of $\Delta\epsilon$. The low concentration of GO flakes stiffen the structure of the 5CB-GO composites. For this reason, the reorientation of \mathbf{n} is more difficult. However, at concentration of 0.2 wt % the material parameters are improved. As the concentration of GO flakes increases, the structure starts to be less uniform than in pure 5CB and a large number of defects makes this composite easier to reorient. Moreover, the director field is disturbed by aggregation of GO flakes.

Table 2: Threshold voltage $U_{th,EO}$ and the calculated results of the splay elastic constants K_{11} in 5CB-GO composites as a function of GO concentration.

wt % of GO	$U_{th,EO}$ [V]	K_{11} [pN]
0	0.80	6.83
0.05	0.83	7.26
0.1	0.77	6.30
0.2	0.72	5.71
0.3	0.74	5.92

At high voltages ($U > U_{th}$), the change of the director reorientation ($U > U_{th}$) from planar to homeotropic alignment and vice versa is characterized by two parameters: the switch-on τ_{ON} and the switch-off τ_{OFF} time. The switch-on time depends on the magnitude of the applied voltage U as follows: $\tau_{ON} = \gamma d^2 / (\epsilon_0 \Delta\epsilon U^2 - \pi^2 K_{11})$, where γ is the rotational viscosity, d is the thickness of the cell and ϵ_0 is the vacuum permittivity. In contrast, the switch-off time is determined mainly by splay elastic constant K_{11} , $\tau_{OFF} = \gamma d^2 / (\pi^2 K_{11})$. After removing the electric field, the director \mathbf{n} relaxes to the initial state due to the elastic nature of the medium. Figure 7 present the dynamic response of the liquid crystal cells filled with different GO suspensions. When the voltage ($U = 10$ V) is turned on, the transmission intensity decreases over time (Figure 7a). The addition of the GO flakes to 5CB does not change the optical response of the cell. Here, the switch-on time refers to the time between 90% to 10% transmission of light (τ_{90-10}). It was found that τ_{ON} increases with the increase of the GO concentration. The effect can be attributed to the increase of the rotational viscosity γ . Figure 7b illustrates the τ_{OFF} dependence. The switch-off time is the time of the director relaxation after removing an electric signal at a given frequency. In the electro-optical characteristic is the time interval where the normalized transmission intensity at the level of 10% rises to 90% (τ_{10-90}). The corresponding figures clearly depict that the flakes suspended in the nematic host recover to their initial state with different times, slower than the pure nematic liquid crystal, which is caused by the increase of the rotational viscosity due to the presence of the GO flakes.

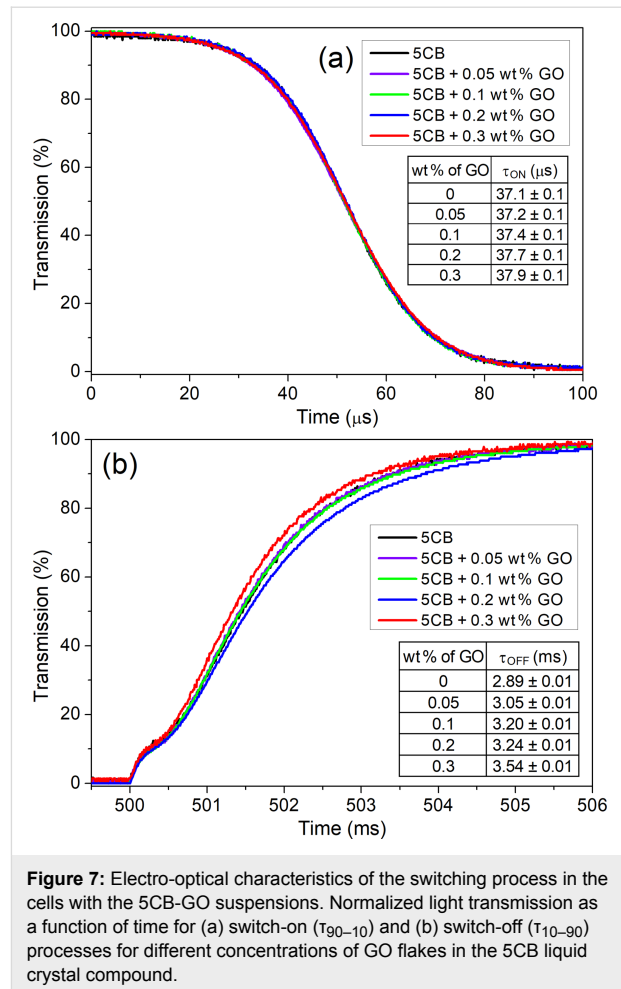


Figure 7: Electro-optical characteristics of the switching process in the cells with the 5CB-GO suspensions. Normalized light transmission as a function of time for (a) switch-on (τ_{90-10}) and (b) switch-off (τ_{10-90}) processes for different concentrations of GO flakes in the 5CB liquid crystal compound.

In the planar oriented cell without the electric field, the GO flakes are suspended parallel to the nematic director \mathbf{n} . At lower concentrations (0.05–0.1 wt %), the nematic order is increased around the GO sheets because of the π - π stacking between the liquid crystal molecules and the GO flakes (Figure 8a). GO flakes stiffen the structure. As the GO ratio increases, the strong π - π stacking induces the deformation of the director field (Figure 8b,c). Moreover, the rotational viscosity increases. At a concentration of 0.3 wt %, the GO aggregates disturb the nematic order significantly. The electric field induces the GO flake/nematic molecule reorientation process. Therefore, in the field on-state, the liquid crystal molecules with GO flakes reorient simultaneously in the field direction (Figure 8d–f). We assume that the electric field destroys the GO aggregates. After turning the electric field off, the distorted director does not accelerate the switching process back to the original orientation. When the electric field is in the off-state, the GO flakes follow the director due to the strong anchoring energy between 5CB's benzene rings and the graphene's honeycomb structure. The interactions between the liquid crystal molecules and the GO flakes are responsible for the lower elastic torque.

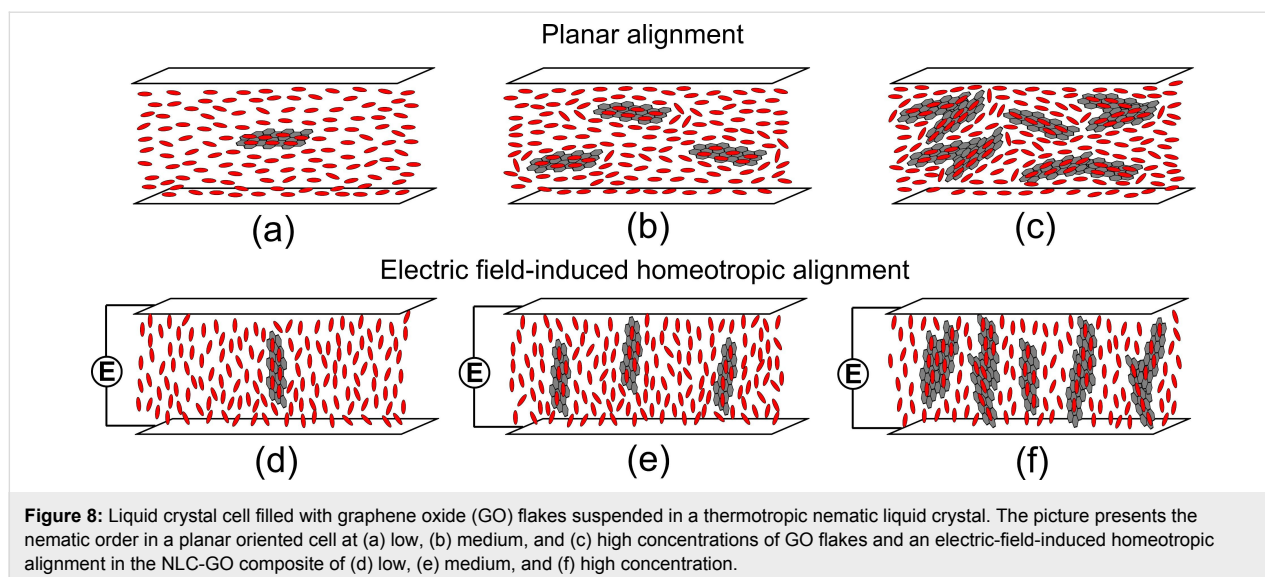


Figure 8: Liquid crystal cell filled with graphene oxide (GO) flakes suspended in a thermotropic nematic liquid crystal. The picture presents the nematic order in a planar oriented cell at (a) low, (b) medium, and (c) high concentrations of GO flakes and an electric-field-induced homeotropic alignment in the NLC-GO composite of (d) low, (e) medium, and (f) high concentration.

Conclusion

We studied the change of the threshold voltage in dielectric spectroscopy and electro-optical measurements of the 5CB nematic liquid crystal with various concentrations of GO flakes (0.05–0.3 wt %). The effect of GO was significant. The reduction of the threshold voltage in the thin liquid crystal cell at the concentration of 0.2 wt % is related to the effects which can be interpreted as the decrease of the elastic constants. In our opinion the reason is related to the alignment of 5CB with respect to the 0.2 wt % GO flakes. When we added more GO flakes, the molecules of 5CB were not aligned properly and the threshold voltage was reduced. It was easier to trigger reorientation of the liquid crystal director when the structure was disrupted as compared to the pure 5CB. Of course, this imperfection in alignment of 5CB molecules is due to the π - π stacking between the 5CB's benzene rings and the graphene oxide's structure. At a low concentration (0.05 wt %) we observed the opposite effect. The structure was stiffened due to the strong interaction of NLC-GO. However, at a higher concentration (0.3 wt %) we noticed the reduction of the threshold voltage because of the significant increase of the rotational viscosity. Nematic liquid crystals with dispersed graphene oxide flakes are interesting candidates for potential applications in liquid crystal modulators and filters, smart windows, and isotropic liquid crystal displays.

Acknowledgements

This work was supported by the Polish Ministry of Science and Higher Education under Mobilność Plus program (grant no. 1644/MOB/V/2017/0), Military University of Technology grant no. PBS 23-652, and the Institute of Electronic Materials Technology (Statutory Research 2018). The authors would like to thank Dr. Adrian Chlanda for the measurements using the

atomic force microscope and Mr. Jerzy Dziaduszek for providing the 5CB compound.

ORCID® iDs

Mateusz Mrukiewicz - <https://orcid.org/0000-0002-0212-4520>

Rafał Mazur - <https://orcid.org/0000-0001-5675-4459>

References

- Li, B.-X.; Borshch, V.; Shiyonovskii, S. V.; Liu, S.-B.; Lavrentovich, O. D. *Appl. Phys. Lett.* **2014**, *104*, 201105. doi:10.1063/1.4879018
- Li, B.-X.; Borshch, V.; Shiyonovskii, S. V.; Liu, S.-B.; Lavrentovich, O. D. *Phys. Rev. E* **2015**, *92*, 050501. doi:10.1103/physreve.92.050501
- Fréedericksz, V.; Zolina, V. *Trans. Faraday Soc.* **1933**, *29*, 919–930. doi:10.1039/tf9332900919
- Yang, D.-K.; Wu, S.-T. *Fundamentals of Liquid Crystal Devices*, 1st ed.; Wiley: Hoboken, NJ, U.S.A., 2006. doi:10.1002/0470032030
- Hsu, C.-J.; Lin, L.-J.; Huang, M.-K.; Huang, C.-Y. *Crystals* **2017**, *7*, 287. doi:10.3390/cryst7100287
- Haraguchi, F.; Inoue, K.; Tushima, N.; Kobayashi, S.; Takatoh, K. *Jpn. J. Appl. Phys., Part 2* **2007**, *46*, L796–L797. doi:10.1143/jjap.46.l796
- Ha, Y.-S.; Kim, H.-J.; Park, H.-G.; Seo, D.-S. *Opt. Express* **2012**, *20*, 6448–6455. doi:10.1364/oe.20.006448
- Sharma, M.; Sinha, A.; Shenoy, M. R. *Opt. Mater.* **2015**, *49*, 292–296. doi:10.1016/j.optmat.2015.09.012
- Reznikov, Y.; Buchnev, O.; Tereshchenko, O.; Reshetnyak, V.; Glushchenko, A.; West, J. *Appl. Phys. Lett.* **2003**, *82*, 1917–1919. doi:10.1063/1.1560871
- Imamaliyev, A. R.; Ramazanov, M. A.; Humatov, S. A. *Beilstein J. Nanotechnol.* **2018**, *9*, 824–828. doi:10.3762/bjnano.9.76
- Lagerwall, J. P. F.; Scalia, G. *J. Mater. Chem.* **2008**, *18*, 2890–2898. doi:10.1039/b802707b
- Javadian, S.; Dalir, N.; Kakemam, J. *Liq. Cryst.* **2017**, *44*, 1341–1355. doi:10.1080/02678292.2016.1278051

13. Dalir, N.; Javadian, S. *J. Appl. Phys.* **2018**, *123*, 115103. doi:10.1063/1.5016388
14. Dalir, N.; Javadian, S.; Kakemam, J.; Yousefi, A. *J. Mol. Liq.* **2018**, *265*, 398–407. doi:10.1016/j.molliq.2018.05.138
15. Basu, R. *Appl. Phys. Lett.* **2013**, *103*, 241906. doi:10.1063/1.4846676
16. Basu, R.; Garvey, A.; Kinnamon, D. *J. Appl. Phys.* **2015**, *117*, 074301. doi:10.1063/1.4908608
17. Chen, H.-Y.; Lee, W.; Clark, N. A. *Appl. Phys. Lett.* **2007**, *90*, 033510. doi:10.1063/1.2432294
18. Basu, R.; Iannacchione, G. S. *Appl. Phys. Lett.* **2009**, *95*, 173113. doi:10.1063/1.3256013
19. Lee, W.; Wang, C.-Y.; Shih, Y.-C. *Appl. Phys. Lett.* **2004**, *85*, 513–515. doi:10.1063/1.1771799
20. Huang, C.-Y.; Hu, C.-Y.; Pan, H.-C.; Lo, K.-Y. *Jpn. J. Appl. Phys., Part 1* **2005**, *44*, 8077–8081. doi:10.1143/jjap.44.8077
21. Huang, C.-Y.; Pan, H.-C.; Hsieh, C.-T. *Jpn. J. Appl. Phys., Part 1* **2006**, *45*, 6392–6394. doi:10.1143/jjap.45.6392
22. Narayan, R.; Kim, J. E.; Kim, J. Y.; Lee, K. E.; Kim, S. O. *Adv. Mater.* **2016**, *28*, 3045–3068. doi:10.1002/adma.201505122
23. Lin, F.; Tong, X.; Wang, Y.; Bao, J.; Wang, Z. M. *Nanoscale Res. Lett.* **2015**, *10*, 435. doi:10.1186/s11671-015-1139-1
24. Kim, J. E.; Han, T. H.; Lee, S. H.; Kim, J. Y.; Ahn, C. W.; Yun, J. M.; Kim, S. O. *Angew. Chem., Int. Ed.* **2011**, *50*, 3043–3047. doi:10.1002/anie.201004692
25. Pei, S.; Cheng, H.-M. *Carbon* **2012**, *50*, 3210–3228. doi:10.1016/j.carbon.2011.11.010
26. Dan, B.; Behabtu, N.; Martinez, A.; Evans, J. S.; Kosynkin, D. V.; Tour, J. M.; Pasquali, M.; Smalyukh, I. I. *Soft Matter* **2011**, *7*, 11154–11159. doi:10.1039/c1sm06418e
27. Tie, W.; Bhattacharyya, S. S.; Gao, Y.; Zheng, Z.; Shin, E. J.; Kim, T. H.; Kim, M.; Lee, J. H.; Lee, S. H. *Nanomaterials* **2017**, *7*, 250. doi:10.3390/nano7090250
28. Tie, W.; Bhattacharyya, S. S.; Lim, Y. J.; Lee, S. W.; Lee, T. H.; Lee, Y. H.; Lee, S. H. *Opt. Express* **2013**, *21*, 19867–19879. doi:10.1364/oe.21.019867
29. Hummers, W. S., Jr.; Offeman, R. E. *J. Am. Chem. Soc.* **1958**, *80*, 1339. doi:10.1021/ja01539a017
30. Boniecki, M.; Gołębiewski, P.; Wesołowski, W.; Woluntarski, M.; Piątkowska, A.; Romaniec, M.; Ciepiewski, P.; Krzyżak, K. *Ceram. Int.* **2017**, *43*, 10066–10070. doi:10.1016/j.ceramint.2017.05.025
31. Dulinska-Molak, I.; Chlanda, A.; Li, J.; Wang, X.; Bystrzejewski, M.; Kawazoe, N.; Chen, G.; Swieszkowski, W. *Micron* **2018**, *108*, 41–48. doi:10.1016/j.micron.2018.02.006
32. Zgłobicka, I.; Chlanda, A.; Woźniak, M.; Łojkowski, M.; Szoszkiewicz, R.; Mazurkiewicz-Pawlicka, M.; Świąszkowski, W.; Wyroba, E.; Kurzydłowski, K. J. *J. Phycol.* **2017**, *53*, 880–888. doi:10.1111/jpy.12548
33. Chlanda, A.; Kijewska, E.; Rinoldi, C.; Tarnowski, M.; Wierzchoń, T.; Swieszkowski, W. *Micron* **2018**, *107*, 79–84. doi:10.1016/j.micron.2018.01.012
34. Urban, S.; Gestblom, B.; Dabrowski, R. *Phys. Chem. Chem. Phys.* **1999**, *1*, 4843–4846. doi:10.1039/a904647j
35. Bogi, A.; Faetti, S. *Liq. Cryst.* **2001**, *28*, 729–739. doi:10.1080/02678290010021589
36. Mrukiewicz, M.; Perkowski, P.; Mazur, R.; Chojnowska, O.; Piecek, W.; Dąbrowski, R. *J. Mol. Liq.* **2016**, *223*, 873–879. doi:10.1016/j.molliq.2016.09.004
37. Hadjichristov, G. B.; Marinov, Y. G.; Petrov, A. G.; Marino, L.; Scaramuzza, N. *J. Phys.: Conf. Ser.* **2016**, *682*, 012015. doi:10.1088/1742-6596/682/1/012015
38. Miller, D. S.; Carlton, R. J.; Mushenheim, P. C.; Abbott, N. L. *Langmuir* **2013**, *29*, 3154–3169. doi:10.1021/la304679f
39. Al-Zangana, S.; Iliut, M.; Turner, M.; Vijayaraghavan, A.; Dierking, I. *Adv. Opt. Mater.* **2016**, *4*, 1541–1548. doi:10.1002/adom.201600351
40. Al-Zangana, S.; Iliut, M.; Boran, G.; Turner, M.; Vijayaraghavan, A.; Dierking, I. *Sci. Rep.* **2016**, *6*, 31885. doi:10.1038/srep31885
41. Burylov, S. V.; Zakhlevnykh, A. N. *Phys. Rev. E* **2013**, *88*, 012511. doi:10.1103/physreve.88.012511
42. Petrescu, E.; Cirtoaje, C. *Beilstein J. Nanotechnol.* **2018**, *9*, 233–241. doi:10.3762/bjnano.9.25

License and Terms

This is an Open Access article under the terms of the Creative Commons Attribution License (<http://creativecommons.org/licenses/by/4.0>). Please note that the reuse, redistribution and reproduction in particular requires that the authors and source are credited.

The license is subject to the *Beilstein Journal of Nanotechnology* terms and conditions: (<https://www.beilstein-journals.org/bjnano>)

The definitive version of this article is the electronic one which can be found at: doi:10.3762/bjnano.10.7